꧂

Solubility of ³He in ⁴He at millikelvin temperatures up to the melting pressure measured by a quartz tuning fork

Elias M. Pentti,[1,][*] Juha T. Tuoriniemi,[1] Anssi J. Salmela,[1] and Alexander P. Sebedash[1,2]

[1]*Low Temperature Laboratory, Helsinki University of Technology TKK, P.O. Box 5100, FI-02015 TKK, Finland*
[2]*Kapitza Institute for Physical Problems, Kosygina 2, Moscow 119334, Russia*

We have studied dilute liquid mixtures of ³He in ⁴He at millikelvin temperatures to find the maximum solubility in the zero-temperature limit, covering for the first time the whole pressure range of the liquid phase. Injecting pure ⁴He into the sample cell through a superleak made it possible to pressurize the mixture up to the melting curve at low temperatures, unattainable through ordinary capillaries due to the minimum of the melting pressure—which would block any customary filling lines at around 1 K. The possibility to selectively drain ⁴He out of the cell through the superleak enabled us to reversibly cover the full span of pressures with a given amount of ³He in the system and to add ³He into the sample volume through an ordinary filling line without the necessity to warm up in between, thus probing the concentration range in small steps in one continuous run in an unprecedented way. Here we report the results on the pressure and temperature dependence of the saturation concentration of the mixture, based on the response of an oscillating quartz tuning fork immersed in the helium mixture. Our data generally agree with earlier results, but suggest that above the solubility maximum around 10 bar the decrease in the saturation concentration as a function of pressure is not as steep as observed in earlier capacitive concentration measurements.

I. INTRODUCTION

The liquid mixture of the two existing stable helium isotopes, ³He and ⁴He, separates below 0.87 K (at saturated vapor pressure) into two phases, one rich and the other dilute in ³He. The solubility of ⁴He in the former phase approaches zero in the limit of low temperatures. However in the latter, ³He has a nonzero solubility even at $T=0$. This property is very important for the entire field of low-temperature physics as it is the basis of dilution refrigeration, which is the only continuously working cooling technique in the millikelvin regime. Moreover, the dilute helium mixture is a fascinating subject of research. At millikelvin temperatures, it consists of two very different components: superfluid ⁴He essentially in its ground state and a degenerate Fermi liquid of ³He. Consequently, the thermodynamics of the mixture are well described by treating the ³He atoms as nearly free fermions with an effective mass between two and three times the atomic mass, in analogy with the free-electron model of metals. It is anticipated that like the electron gas in many metals and the atoms of pure ³He liquid, the dilute ³He system also has a superfluid transition at a yet unknown temperature.[1]

The atom density of ³He in the dilute system, i.e., the concentration, is the primary input parameter for any investigations on helium mixtures, whether experimental or theoretical. To the practical aspect, there is in general no simple way to tell the precise ³He concentration in the sample cell at low temperatures without determining it *in situ*. It is usually not safe to simply assume that the open volume of the low-temperature cell has exactly the same proportion of ³He as the sample gas at room-temperature storage tanks—which, for that matter, is not trivial to keep track of in the first place. The thermal gradients in the filling capillaries, although having very small volume usually, give rise to large concentration gradients due to the osmotic pressure effects. Also, the

low-temperature assemblies must include heat exchangers, standardly made of sintered fine metal powder, where the very small open volumes and huge surface areas potentially alter the conditions from the bulk due to the stronger binding energy of ⁴He to surfaces. For theoretical work, it is of utmost importance to know the limiting concentration in order to pin down the mixture properties, as the solubility does depend on the mutual interactions between the quasiparticles.

In this paper, we report the first use of a quartz tuning fork to monitor the concentration of a dilute helium mixture directly in the low-temperature experimental cell. By this method, we have determined the saturation concentration of ³He in the mixture in the zero-temperature (zero-*T*) limit across the complete pressure range. In particular, we have collected data at the melting pressure of ⁴He in the saturated mixture (25.64 bar) where cooling of the mixture by adiabatic melting of ⁴He can be performed.[2,3] Earlier published data do not extend up to the melting pressure although the saturation concentration has been measured at lower pressures by various techniques over the last four decades.[4–8] We also determined the coefficient of the quadratic temperature dependence of the saturation concentration at various pressures.

Quartz tuning forks are mass produced components intended for frequency standards in electronics, and they have been introduced relatively recently as oscillating probes for the helium research.[9,10] Other kinds of mechanical oscillators have routinely been employed in this field for a variety of purposes,[11–15] but an obvious advantage of the quartz forks is that they can be purchased in great numbers for a negligible price in a form nearly ready to use. Forks of a certain type are practically identical and could, therefore, be used as detectors in different laboratories with only minor correction of parameters. Moreover, magnetic field is neither necessary for

the operation of the forks nor does it affect them. On the other hand, the relation between the resonance characteristics of the oscillating fork and the properties (such as density and viscosity) of the surrounding fluid is not known analytically due to the nontrivial geometry.

The method of measuring the density or concentration of a helium mixture by means of an immersed oscillator is based on detecting the change in the mechanical resonance frequency resulting from the mass of the liquid being forced into motion together with the probe itself. Quartz tuning forks are superior for this purpose for two main reasons: first, their lower density compared to metallic oscillators makes them more sensitive to the density of the surrounding fluid, and second, their intrinsic properties are essentially immune to changes in temperature and pressure across the ranges covered. Empirical background calibrations due to changes in these variables are needed, for example, when using the capacitive method, as is customary for the precision measurements of the densities of helium liquids.

In the capacitive method, which has been dominant in previous concentration measurements, the total number density of helium atoms is first calculated by the Clausius-Mossotti relation from the capacitance of a pair of electrodes with mixture in between, and thereafter the ^{3}He concentration is deduced by the fact that in a helium mixture an atom of ^{3}He occupies more space than ^{4}He due to larger zero-point motion so that the molar volume of the mixture increases with ^{3}He concentration. In our method, probing of the mass density instead of number density enhances sensitivity of the measured quantity to concentration because ^{3}He atoms do not only occupy more space but also, naturally, weigh less by a factor very precisely known.

Another key component of our experimental setup, in addition to the quartz tuning fork, is a superleak filling line in parallel with a customary filling capillary to the sample cell. That made it possible, first, to scan the full range of pressures where dilute helium mixtures remain liquid at millikelvin temperatures, and second, to increase the ^{3}He concentration of the sample in small steps from zero to saturation in one continuous run thus covering the whole parameter space of liquid mixtures. Taking advantage of the pressure and temperature dependence of the saturation concentration, we also produced metastable supersaturated mixtures.

The remaining of this paper is organized as follows: Section II describes the experimental setup and the techniques, and Sec. III describes the considerations related to the analysis of the behavior of the quartz oscillator immersed in helium fluids. The pressure and temperature dependencies of the saturation concentration of the mixture are presented in Secs. IV and V followed by some discussion in Sec. VI. The paper is closed by a short summary.

II. EXPERIMENT

A. Apparatus

The experimental volume consisted primarily of a cylindrical cell mounted on the mixing chamber of a dilution refrigerator. The geometry was somewhat more complicated due to the integration with a capacitive pressure transducer
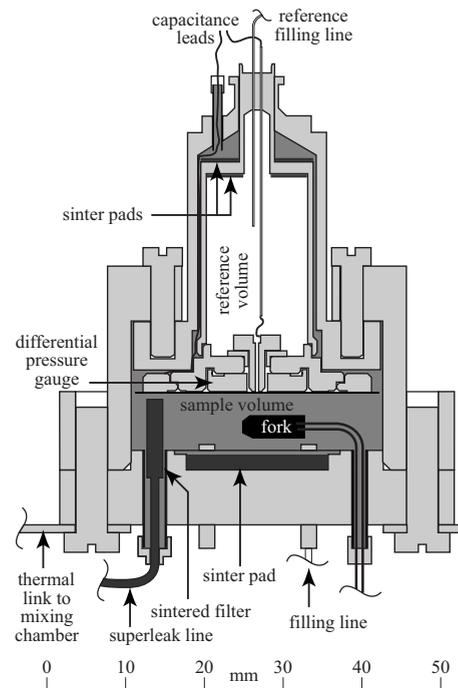

FIG. 1. Cross section of the experimental cell. The mixture sample occupies the space presented in medium gray surrounding the reference volume of the differential pressure gauge.

with a separate reference volume filled by pure ^{4}He. Figure 1 shows the cross section of the low-temperature assembly.

Two sensors were mounted for probing the properties of the helium mixtures: a quartz tuning fork (described in detail in the next subsection) and a capacitive differential pressure gauge suitable for accurate measurements of the crystallization pressures of the mixtures.[16,17] The differential gauge measures, by means of a flexible BeCu membrane, the pressure difference between the sample and the reference volume. For melting curve measurements, the pure ^{4}He in the reference volume was partly solidified to provide a stable reference pressure independent of temperature at the range of interest.

The measured size of the sample volume was $V_{cell} = (8.3 \pm 0.2)$ cm^3 at room temperature. Unfortunately, it is difficult to determine that very precisely either by experiment or from the geometry. The actual shape is quite complicated and the pads of sintered silver powder may contribute to the effective volume by an unknown factor. There were separate sinters for thermalizing the sample and the reference volume with the cell wall.

Besides a conventional filling capillary to the sample volume, there were three parallel superleak lines—capillaries tightly packed with fine powder. There were several such lines with varying packing conditions for testing purposes. However the one with the best performance was exclusively used in the present study. Therefore, in the schematic diagram of the setup in Fig. 2 only one superleak is shown. The superleak lines were about 3 m long with a diameter of about 1 mm and their upper ends were held at about 1.5 K to have liquid superfluid phase there at all times. When operating at the proximity of the melting pressure, these lines could be
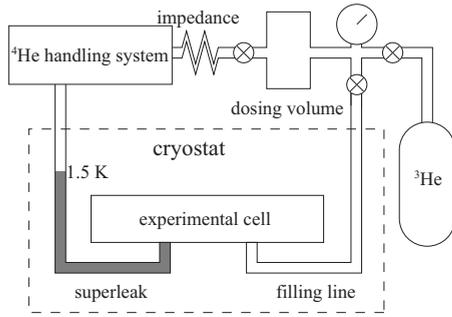
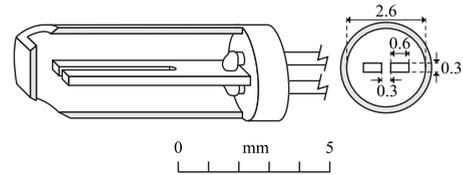FIG. 2. Schematic diagram of the filling lines.

FIG. 3. On the left: a perspective view of the quartz tuning fork in its casing depicted with the front half cut away. On the right: The cross section of the casing and the fork with dimensions in millimeters.

closed at will by letting the upper end cool closer to 1 K—whereby solid ^{4}He blocked the lines. One of the superleak lines was actually totally blocked and thus unusable from the beginning of the experiment. Nevertheless, their lower ends were connected to the sample volume, which is made volumetry by using pure liquid ^{4}He unreliable.

For the present study, the superleaks have two important properties. First, ^{4}He confined in the pores of the superleak has a melting pressure higher than that of the bulk liquid. Therefore, in spite of the minimum of the melting curve of mixtures at about 1 K, causing the customary filling lines to block before creating solid into the cell, the mixture in our experiment could be pressurized up to its solidification limit in the millikelvin regime by simply adding ^{4}He through the superleak. Second, as the superleak allows only superfluid ^{4}He to pass, it made it possible to gradually increase the ^{3}He content of the cell without warming up by injecting ^{3}He through the ordinary filling line and removing a corresponding amount of ^{4}He through the superleak. In the course of the measurements, this process was repeated in roughly constant steps many times. We quantified each addition of ^{3}He by taking a pure ^{3}He gas dose to a specific room-temperature volume, the pressure of which was accurately measured before releasing the dose into the filling line of the cell. Then we thoroughly flushed the system by pure ^{4}He to ensure that all the ^{3}He in the filling line found its way into the cell. Backward flow of ^{3}He into the ^{4}He handling system was prevented by a flow impedance shown in Fig. 2. Once it arrived in the cell, ^{3}He preferably remains there because the osmotic pressure in the superfluid background drives it to the parts with the lowest temperature. Twenty additions saturated our sample at low pressures and a total of 33 were needed to have a saturated mixture at all pressures below melting. Of course, checks were made along the way to observe if any appreciable amount of ^{3}He was lost in the course of the experiment.

The pressure of the cell was controlled by changing the amount of ^{4}He in it, always adding through the ordinary line (except when the pressure was so high that the ordinary line was blocked by solid) and removing through the superleak line in order to ensure that all the ^{3}He remained in the cell. Because of this method, with a certain amount of ^{3}He in the cell, measurements at different pressures were made at equal partial densities of ^{3}He, not at equal concentrations. The sample pressure was usually measured by a piezoelectric pressure gauge on the ordinary filling line at room tempera-

ture. When the line became blocked before reaching the solidification pressure in the cell, filling was continued through the superleak line, and the internal capacitive pressure gauge was employed.

The temperature of the experimental cell was mainly monitored by a carbon resistor in the mixing chamber calibrated against a ^{60}Co nuclear orientation thermometer in the millikelvin regime and against a commercial calibrated Ge resistor at higher temperatures. In addition, the temperature of the cold plate of the mixing chamber and thus of the body of the experimental cell was measured by a Pt-NMR thermometer. Yet, most direct indication of the temperature of the sample liquid was obtained by the immersed quartz fork in a manner explained below. It was then easy to observe any significant deviations from equilibrium and eliminate any transient effects from the analysis.

B. Quartz tuning fork

Quartz tuning forks can be purchased from several suppliers in somewhat varying sizes and physical mounting. Most have been designed to respond at 2^{15} Hz, at room temperature, for clocking purposes. The single-crystal quartz oscillators with evaporated driving electrodes on their surface are hermetically sealed to provide better precision and stability. This seal must be broken one way or the other in order to use them for the present purpose.

The quartz tuning fork used in our experiment was of type NC38 from Fox Electronics.[18] The fork was left in its original metal casing, which was opened by grinding two holes at the end of the cylindrical cover. Figure 3 shows the fork casing in a cutaway drawing and in a cross-sectional view, and Fig. 4 shows a photograph of a fork, identical to the one employed in the experiment but with the cover completely removed.
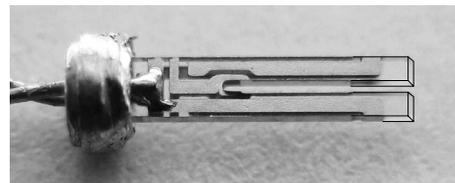

FIG. 4. Photograph of a quartz tuning fork of the type used in the experiment; the cylindrical cover has been completely removed. The ends of the quartz tines, to the right, have been outlined by black lines to improve visibility. The electrodes for the piezoelectric drive can be seen on the surface. Photograph was done by Rysti.

The electromechanical fork resonance was measured by standard laboratory equipment. We excited the quartz crystal by a computer-controlled digital function generator and detected the signal by a lock-in amplifier—see Ref. 19 for details of the measuring circuit. Excitation was kept to a level much below the limit where the oscillator starts to deviate from linear response. Therefore, the fork behaves as a damped harmonic oscillator with an approximately Lorentzian resonance peak characterized by the resonance frequency f_0 and the peak width Δf_2 (full width at half maximum). These two carry information on the properties of the fluid surrounding the fork and were determined either by fitting an analytic curve to a spectrum with some tens of data points spanning several peak widths around the resonance or by calculating them from the signal measured at a single point near the resonance. The single point method is much faster and can be used once a calibration spectrum has first been measured and analyzed to obtain the background and the phase of the signal and the invariant product of the height and the width of the peak. The consistency of the adopted parameters was frequently checked and they were found to hold remarkably well in spite of varying conditions throughout the experiments. The resonance frequency of our fork in vacuum at liquid helium temperatures was 32 738.327 Hz, slightly less than the nominal 32 768 Hz because of reduced temperature but stable within the limits of observability and independent of temperature in the experimental range. The statistical error of the measurements was of the order of 1 mHz, but the long term stability was limited by the performance of the room-temperature electronics to some 10^{-7}. In terms of properties of the helium mixture, the resolution of the fork measurement was of the order of 1 mbar in pressure and 10 ppm in ^{3}He concentration.

III. ANALYSIS OF THE IMMERSED OSCILLATOR

The resonance characteristics of a mechanical oscillator immersed in liquid helium mixture depend on all variables defining the state of the surrounding fluid: pressure, temperature, and concentration (particle density). Although the quartz tuning forks may be employed to measure any of the three, once the other two have been determined by other means, we shall focus on the concentration problem—which is probably the technique least developed. The resonant frequency of the fork depends on the inertia added to the oscillatory motion by the fluid, whereas the width of the resonance peak results from damping (quasiparticle scattering). The presence of ^{3}He in the mixture affects both.

A. Idealized medium

The resonance frequency f_0 of an oscillating body immersed in an inviscid and incompressible fluid is shifted from the vacuum value $f_{0,\text{vac}}$ according to

$$\left(\frac{f_{0,\text{vac}}}{f_0}\right)^2 = 1 + B\frac{\rho_{\text{liq}}}{\rho_{\text{body}}}, \qquad (1)$$

where ρ_{liq} and ρ_{body} are the densities of the liquid and the body, respectively, and B is a geometrical factor of order

unity. For example, for an infinitely long single cylinder in an unbounded volume one has $B=1$ exactly. In our case, the oscillating body is one of the tines of the fork with density ρ_{fork} and the liquid is a dilute mixture of ^{3}He in ^{4}He. The density of the dilute mixture can be expressed as

$$\rho_{\text{mix}} = \frac{M_4}{v_4} - n_3[(1+\alpha)M_4 - M_3], \qquad (2)$$

where v_4 is the molar volume of pure ^{4}He, M_3 and M_4 are the molar masses of the isotopes, n_3 is the molar density of ^{3}He, and α is the BBP parameter named after Bardeen, Baym, and Pines[20] (the developers of the theory of helium mixtures). Now, substituting the relevant densities in Eq. (1) yields

$$\left(\frac{f_{0,\text{vac}}}{f_0}\right)^2 - 1 = \frac{BM_4}{\rho_{\text{fork}}v_4} - \frac{B[(1+\alpha)M_4 - M_3]}{\rho_{\text{fork}}}n_3. \qquad (3)$$

This relation, in principle, enables the calculation of n_3 in a mixture when f_0 has been measured, since the ratio B/ρ_{fork} can be fixed by a measurement in pure ^{4}He, in other words with $n_3=0$, and all other factors are known from literature. The obtained n_3 immediately gives the ^{3}He concentration x through

$$x = \frac{n_3 v_4}{1 - \alpha n_3 v_4}. \qquad (4)$$

For the evaluation of α at different pressures, we use a phenomenological formula based on Ref. 5,

$$\alpha = 0.325\,92 - 0.062\,49 \ln\left(\frac{p}{\text{bar}} + 4.505\,59\right), \qquad (5)$$

and we adopt the values of v_4 at different pressures from Tanaka *et al.*[21] In practice, however, the picture is complicated by the fact that the helium mixture is both compressible and viscous to a significant extent.

B. Effect of compressibility

The fact that the medium is compressible complicates the data analysis by introducing additional pressure dependence to the observed frequency shifts. Fortunately, this contribution is still relatively small in helium liquids with the dimensions and the frequency of the quartz forks and it can be accounted for by letting the parameter B, which is otherwise a geometrical constant, to depend on the speed of sound of the medium and thus pressure. We shall show that the effect across the whole pressure range at low temperatures is of the order of 5% in the calculated density, which is easily observable. This effect can be studied by making measurements in pure liquid ^{3}He and ^{4}He, where the densities are well known. As described below, the complication can be largely circumvented by the appropriate treatment of the data.

Another phenomenon due to finite compressibility is the appearance of second sound resonances in mixtures when the wavelength of the sound modes matches some dimensions of the resonator. We observed strong attenuation peaks above and below 1 K, where the speed of second sound has its

broad maximum.[22] These resonances obscure much of the data in mixtures at higher temperatures but the situation settles down at millikelvin temperatures because the temperature dependence of the speed of second sound eventually flattens out to a value that varies only little with pressure or concentration. The observed resonances bear interest on their own but for the present study their appearance was just a nuisance.

Both these effects would become smaller by reducing the size of the oscillator, while the frequency is pretty much fixed to its standard value for as long as commercial forks are used. Let us describe this problem in some more detail.

As noted, the compressibility of fluid gives rise to sound or propagation of density waves. As the propagation of sound is adiabatic, it also involves a variation of temperature. In dilute helium mixtures, there are two normal modes of sound waves: in the first mode, the densities of ³He and ⁴He components oscillate in the same phase; this mode is called first sound and this corresponds to "normal" sound in air, say. In the second mode, the densities oscillate in opposite phases, which implies propagating minima and maxima of ³He concentration; this is called second sound. It also occurs in pure superfluid ⁴He, where the two oscillating components are the superfluid and the normal liquid.

In their theoretical presentation of first and second sounds in dilute helium mixtures, Brucker *et al.* [Eqs. (25)–(27) of Ref. 23] provide a system of three linear homogeneous equations for the (relative) oscillation amplitudes of the three variables of a mixture: temperature and the densities of ³He and ⁴He. We do not intend to make any quantitative calculations on the basis of their equations, but we draw a couple of important qualitative conclusions. The velocity of sound S appears in the coefficient matrix of the system in such a way that the determinant is a quadratic polynomial of S^2. Thus, the system has nontrivial solutions for two positive values of S at which the determinant vanishes; these are the velocities of first and second sounds. Furthermore, in a given mode, the oscillation amplitude of one of the three variables fixes the other two. From our point of view, this has the important consequence that an impenetrable body vibrating in the mixture excites both sound modes because, at the surface of the body, the amplitudes of the displacements of the two components of the liquid must be equal. In general case, pure first sound does not satisfy this condition but a superposition of both modes is necessary.

The significance of compressibility effects can be estimated by comparing the dimensions of the oscillator with the wavelength of sound. The velocity of second sound in a saturated mixture at millikelvin temperatures is roughly 15 m/s,[24] which means that at frequencies close to 30 kHz the wavelength is about 0.5 mm, comparable to the dimensions of the fork. In other words, the density of the surrounding liquid inevitably varies in the length scale of the oscillator, and, moreover, the resonant modes of second sound inside the fork container are possible.

Our results in pure ⁴He at millikelvin temperatures where the normal liquid density and thus second sound effects are negligible and in pure normal ³He, indicate that compressibility plays a role even when second sound is absent—despite that the velocity of first sound in ⁴He (³He) varies
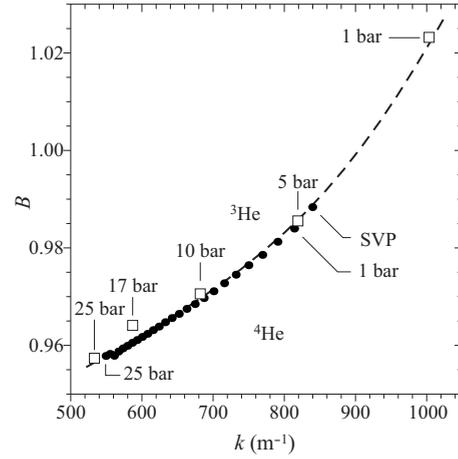

FIG. 5. B as a function of wave number in pure ³He (□) and ⁴He (●) liquids at indicated pressures. We have used ρ_{fork} =2.659 g/cm³ here. The dashed line is a guide to the eye.

between 240 (190) and 360 (380) m/s as a function of pressure in the studied range.[19] Figure 5 presents values of B calculated by Eq. (1) from fork measurements in the pure isotopes at different pressures plotted as a function of wave number $k = \omega/c$, where ω is the angular resonance frequency of the fork (in ³He the extrapolated value in the inviscid limit, see below) and c is the velocity of sound. Sound velocity in pure ³He is calculated from the zero-temperature molar volume data in Table IX of Ref. 25, and in pure ⁴He it is calculated from the molar volume of Ref. 21. Both data appear to have the same dependence on k although the densities of the two media differ considerably. Due to second sound effects in the mixtures, we cannot take for granted, however, that the same dependence applies there as well.

C. Effect of viscosity

The ³He component in the mixture is rather viscous at millikelvin temperatures so that the immersed vibrating fork experiences a drag force, which decreases its resonance frequency further from the corresponding value in an inviscid liquid and also greatly widens the resonance peak. As the viscosity in this regime varies as T^{-2}, it could be varied over a couple of orders of magnitude in our experiment by changing the temperature. This, most naturally, provides means for thermometry if the conditions are otherwise kept constant,[9] as also referred to earlier in this text.

Figure 6 shows a graph of the width versus the frequency of the fork resonance in an almost saturated helium mixture at a pressure of 13 bar and temperatures between 7 and 40 mK. From 10 mK up to about 30 mK the data follow closely a straight line with slope −4, a property common to all concentrations and pressures in our study. The steepening of the curve at the lowest temperatures results from slip effects due to increasing mean free path of the quasiparticles;[26] the hump below 40 mK is a broad second sound resonance and the excursion from the line at higher temperatures indicates emergence of further resonances and other effects related to increasing temperature.
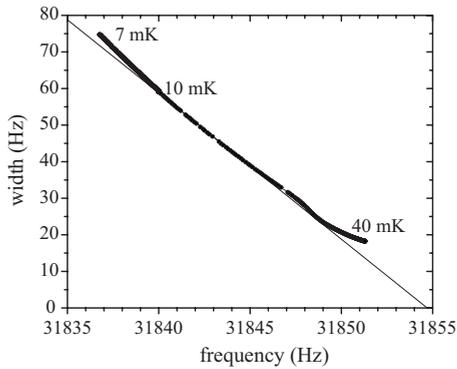
FIG. 6. Data of the quartz fork in a mixture near saturation at 13 bar between 7 and 40 mK, and a line with slope −4.

The universal slope of −4 in such graphs, or at least values very close to that, is common also to other types of oscillators in helium mixtures, such as bent vibrating wire resonators.[27] We can use this empirical fact to eliminate the viscosity effect from the fork data by defining a quantity $\tilde{f}$ $=f_0+\Delta f_2/4$ (with f_0 and Δf_2 being measured with the mixing chamber at about 10 mK) as an approximation of the resonance frequency of the fork in an inviscid liquid, and use that value when calculating densities of mixtures. Because of second sound effects and thermal expansion at hundreds of millikelvins where the viscosity is significantly lower, a more accurate determination of the inviscid limit is not feasible. At this chosen measuring temperature, the saturation concentration is already very close to the zero-temperature value, the relative difference being less than 10^{-3}.

IV. ZERO-*T* LIMIT OF SOLUBILITY

When the amount of ^{3}He in the system was sufficient to saturate the mixture at low pressures but not enough to keep it so at higher pressures because of the increase in solubility and addition of ^{4}He for pressurization, it was easy to observe the point where the solution departed from the saturation curve as a kink in the fork data as a function of pressure. If we can rely on our bookkeeping of the ^{3}He content, this immediately gives one point on the saturation curve in the concentration-pressure diagram.

Instead, we adopted a somewhat more complicated procedure to analyze the data. It would indicate any appreciable loss of ^{3}He from the system, makes no presumptions upon the parameter B/ρ_{fork} of Eq. (3), and gives the limiting solubility basically at an arbitrary value of pressure. The last point was of importance particularly at higher pressures where the solubility curve slopes quite gently down and now the need to decrease the pressure and, thus, to remove ^{4}He opposed this trend and made the departure from the saturated condition nearly unnoticeable.

Ideally, at any value of pressure the inverse square of the inviscid resonance frequency is linear in N_3, the amount of ^{3}He in the mixture [as is obvious from Eq. (3)]. Plotting the left-hand side as a function of N_3 at various pressures would produce a family of straight lines where the whole pattern just scales according to the parameter B/ρ_{fork} and everything
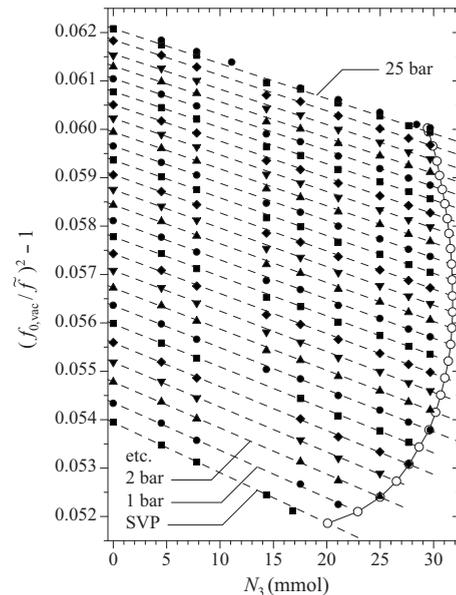

FIG. 7. Data used to empirically find the relation between the response of the fork and the amount of ^{3}He in the system and thereby to determine the saturation value of ^{3}He content. ○: saturation, solid symbols: homogeneous mixtures, dashed lines: linear fits to data at each pressure.

else is known. In our experiment the pressure was swept regularly up and down after each few additions of ^{3}He so that we can compile such a plot by picking data values at certain pressures from each recursion. We present these data in Fig. 7 together with fitted lines and the saturation values of N_3, obtained as the points where the linear fits intersect the values observed in the saturated mixture. Now we can critically inspect the deviations from the ideal picture.

First of all, the inverse square of the inviscid resonance frequency is still to a good approximation linear in N_3 despite the complications arising from finite compressibility. This is rather natural, as any other result would require serious departure of the k dependence of B in mixtures from what we observed in the pure liquids. The points where the lines meet $N_3=0$ can be used to produce a plot such as that in Fig. 5 if the p dependence of the molar volume of pure ^{4}He is assumed to be known. If there was nothing more to the problem, then also the slopes of the lines would be fixed by the very same parameter. However, our data showed that the reality is not quite that simple. The fitted slopes, multiplied by the estimated cell volume, are plotted in Fig. 8 together with the behavior expected on the basis of the data in the limit of pure ^{4}He. There is a good resemblance between the data and the proposed curve, but the data systematically lie somewhat above the curve, more so at the lowest pressures. This could indicate, for one thing, that α deviates from the form proposed in Eq. (5). The needed adjustment can be read from Fig. 8 by means of the dashed lines that indicate constant values of α and define an alternative, slightly curvilinear coordinate system in which the theoretical curve is the graph of Eq. (5). The measured points give the values of α needed to reproduce the experimental data. At zero pressure, for example, this interpretation suggests $\alpha \approx 0.33$. We con-
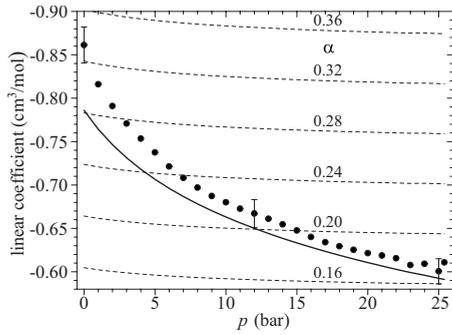
FIG. 8. The observed slopes of the dependence of $(f_{0,\mathrm{vac}}/\tilde{f})^2$ on the density of ^{3}He in the cell (bullets) and the slope calculated by Eq. (3) (solid curve). The dashed lines present calculated slopes at indicated constant values of α. The error bars shown are representative to all data and result from the uncertainty of the volume occupied by the added ^{3}He.

FIG. 9. Saturation concentration of helium mixture relative to the zero pressure value: (■): Our data (10 mK), (△) Watson's data (Ref. 5) (50 mK), (◇) Landau's data (Ref. 6) (zero-T limit), and (○) Yorozu's data (Ref. 7) (zero-T limit, measurement dependent on Watson's data).

clude that the correction necessary for explaining the experimental behavior is unacceptable, especially at the lowest pressures where the previous experimental data available are probably most precise. Therefore, we are led to believe that the observed mismatch is rather caused by additional degrees of freedom in the system, most likely due to the second sound.

Finally, we are ready to present the results on low-temperature solubility of ^{3}He in ^{4}He. The amount of ^{3}He needed to saturate the mixture at any pressure can be read from Fig. 7. In order to convert the known amount of ^{3}He in the system to absolute values of concentration, we need to know the volume occupied by the added ^{3}He at low temperature. Unfortunately, this is inevitably somewhat ambiguous due to the unknown contribution of the sinters and because some of the ^{3}He is distributed to the filling capillary. Nevertheless, it is reasonable to assume that their influence scales with the total amount of ^{3}He in the system and so each addition of ^{3}He increases the content of interest by the same proportion each time. Therefore, we obtain the relative saturation concentration as a function of pressure very precisely from this data, although the absolute scale remains somewhat more inaccurate. The single reference point may be chosen to be any, but the most obvious one is the saturation concentration at the saturated vapor pressure (practically $p=0$). The relative solubility data are shown in Fig. 9 together with the results of three preceding studies, scaled to represent the data in a similar fashion.

The four data sets in Fig. 9 agree fairly well below the solubility maximum at about 10 bar—especially ours and that of Landau *et al.*[6] who measured the saturation concentration through the osmotic pressure of the mixture. Above maximum the data differ more from each other. The decrease in the solubility is steeper according to the two measurements made by the capacitive method (Watson *et al.* and Yorozu *et al.*) than that suggested by the other two. It appears plausible that the capacitive method may have some systematic error at high pressures, which the latter authors have inherited from the former. Namely, in their footnote 11, Yorozu *et al.* stated that they actually used Watson's data to calibrate their concentration gauge after unexplained jumps
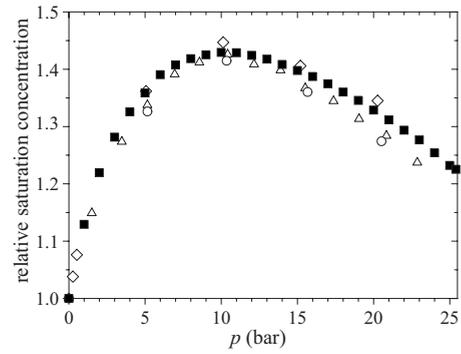
of the capacitance. Conceivable sources of a pressure-related systematic error include the sensitivity of the capacitors to pressure, not properly accounted for, and the dependence of the method on the knowledge of the BBP parameter α, which describes the difference of the molar volumes of the ^{3}He and ^{4}He components in the mixture. In our method the sensor is undoubtedly immune to external pressure at this range and the effect of α is not a critical factor because the oscillator senses the mass density and not just the number density.

For further reference, Table I is a list of our experimental values at pressures ranging from the saturated vapor pressure (essentially zero) to the melting pressure of the saturated mixture, 25.64 bar. Concentration at the highest pressure could not be determined because our method of analysis requires measurements at some lower concentrations and they have lower melting pressures. We tabulate the fork resonance frequencies in pure ^{4}He and in the saturated mixture (extrapolated to zero viscosity) and the saturation concentrations relative to the value at zero pressure. Once the zero pressure value is agreed upon, the whole curve can immediately be put into the absolute scale. The proposed readings for this range from 6.5% to 6.8%. If we choose, somewhat arbitrarily, the reference point to be 6.65% at 0 bar, the other "strategic" values would read 9.50% for the maximum of solubility at 10 bar and 8.12% at the melting curve. If we blindly use the volume we determined for our experimental cell, we obtain values somewhat higher than these: 6.8%, 9.7%, and 8.3%, respectively. For completeness, we plot in Fig. 10 the absolute readings using our cell volume. The error margins displayed are entirely due to the uncertainty in this volume.

V. SOLUBILITY AT FINITE TEMPERATURES

The first approximation due to finite temperature for the saturation concentration of the mixture is usually written as

$$x_s(p,T) = x_s(p,0)[1 + \beta(p)T^2]. \tag{6}$$

The pressure dependence of the factor β was earlier investigated by Yorozu *et al.*[7] using the capacitive method. We examined this by two procedures: by temperature sweeps at

TABLE I. Measured resonance frequencies in pure ^{4}He and saturated mixture, and the obtained relative saturation concentrations. The estimated error of the relative concentration is ± 0.003.

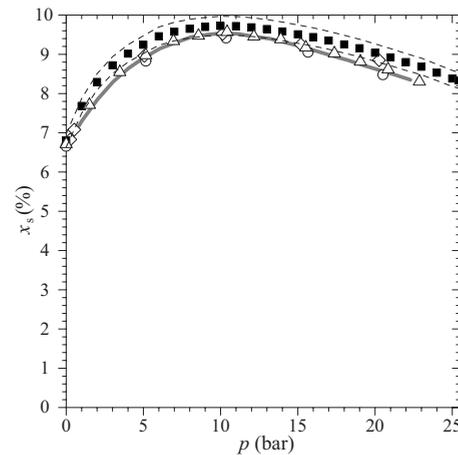| p (bar)	$\tilde{f}$ (Hz)		$x_s(p)/x_s(0)$
	Pure ^{3}He	Saturation	
0	31889.44	31921.1	1.000
1	31883.55	31917.5	1.129
2	31876.87	31912.9	1.220
3	31870.71	31907.9	1.282
4	31864.55	31902.6	1.326
5	31858.65	31897.2	1.359
6	31852.97	31891.9	1.390
7	31847.51	31886.4	1.408
8	31842.14	31881.0	1.418
9	31836.88	31875.6	1.425
10	31831.65	31870.4	1.429
11	31826.67	31865.2	1.429
12	31821.73	31860.1	1.424
13	31816.97	31855.0	1.418
14	31812.41	31850.0	1.408
15	31807.85	31845.1	1.398
16	31803.47	31840.2	1.387
17	31799.11	31835.3	1.375
18	31794.87	31830.6	1.360
19	31790.69	31826.0	1.346
20	31786.66	31821.4	1.329
21	31782.66	31816.9	1.312
22	31778.88	31812.6	1.294
23	31775.41	31808.1	1.277
24	31770.84	31803.5	1.254
25	31767.12	31799.1	1.232
25.4	solid	31797.9	1.225
25.64	solid	31796.4	

FIG. 10. Saturation concentration of helium mixtures. ■: Our data (10 mK); △ and gray curve: Watson (Ref. 5) measured points and tabulated smooth data (50 mK); ◇: Landau's data (Ref. 6) (zero-T limit); and ○: Yorozu's data (Ref. 7). Dashed curves represent the error bounds of our data due to the uncertainty of the cell volume.

constant pressure and by pressure sweeps at constant temperature. We exploited the fact that the system with just a small amount of pure ^{3}He can be brought into a state of supersaturation to a certain extent by suitably varying either pressure or temperature. This way we obtained two alternative curves for the fork response: one with a homogeneous supersaturated state and the other with the phase separated state having the saturation concentration of the mixture around the fork. With a given amount of ^{3}He in the cell, the supersaturated state always had a constant partial density of ^{3}He due to our method of measurements and it provided a nearby reference curve for the saturated case to be compared with.

A. Temperature sweep

The temperature sweep proceeded as follows: With the amount of ^{3}He and the pressure such that at the lowest tem-

peratures there was a small amount of pure ^{3}He in the cell, we first warmed the sample slowly up to a temperature sufficient to remove the phase separation, usually in the range 70–200 mK. The warming was paused at a few temperatures to establish the relation between the fork resonance width and the temperature so that the fork signal could serve as a thermometer in addition to indicating the concentration. Then we cooled the sample down again and it remained in the homogeneous supersaturated phase until the pure ^{3}He phase nucleated at a temperature notably lower than that needed for complete mixing. Between the points of complete dissolution of the pure ^{3}He phase and its nucleation, we obtained two different fork responses: one for the saturated mixture during the warming and the other for a supersaturated mixture with some constant concentration X during the cooling.

As an example, a temperature sweep measurement at 11 bar is shown in Fig. 11. The two states of the system can be clearly distinguished over a certain range of temperatures (resonance widths). The loops and bends in the high-temperature end of the data resulted from resonant absorption of second sound. The difference of the fork resonance frequencies at a certain width denotes the difference of the concentrations at the corresponding temperature. Using the established temperature dependence of the fork resonance width, we compute the difference of the inverse squares of the fork resonance frequencies as a function of T^2—the data thus computed for the measurement at 11 bar is shown in Fig. 12. We then fit a straight line to the linear part of the graph to find the derivative,

$$\begin{aligned} D &= \frac{d(f_0^{-2}(X,T) - f_0^{-2}[x_s(T),T])}{d(T^2)} \\ &= \frac{\partial f_0^{-2}(X,T)}{\partial(T^2)} - \frac{\partial f_0^{-2}(x_s,T)}{\partial(T^2)} - \frac{\partial x_s(T)}{\partial(T^2)}\frac{\partial f_0^{-2}(x_s,T)}{\partial x_s}. \end{aligned} \quad (7)$$

The first two terms approximately cancel out because $X \approx x_s$ throughout the measurement so that
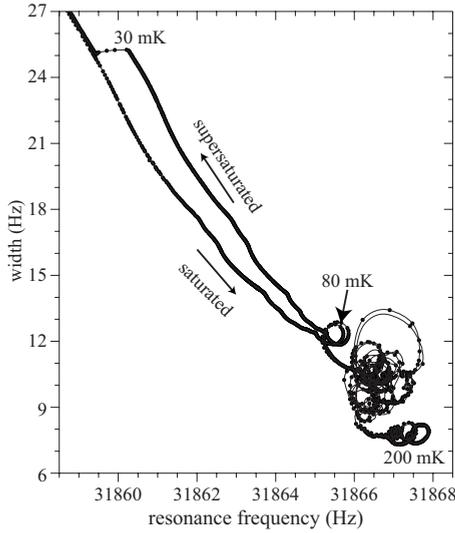
FIG. 11. Fork response during warming and cooling of a mixture at 11 bar. The arrows indicate the direction of time. The supersaturated state could be maintained between about 30 and 100 mK.

$$D \approx -\frac{\partial f_0^{-2}(x)}{\partial x}\frac{\partial x_s(T)}{\partial(T^2)} \approx -\frac{\widetilde{f}^{-2}[x_s(0)] - \widetilde{f}^{-2}(0)}{x_s(0)}\frac{\partial x_s(T)}{\partial(T^2)},$$
(8)

where the former derivative has been replaced by the difference quotient calculated from the values of the inviscid resonance frequencies in the saturated mixture, $\widetilde{f}[x_s(0)]$, and in pure ^{4}He, $\widetilde{f}(0)$. On the grounds of Eq. (6) we obtain

$$\beta = \frac{D}{\widetilde{f}^{-2}(0) - \widetilde{f}^{-2}[x_s(0)]},$$
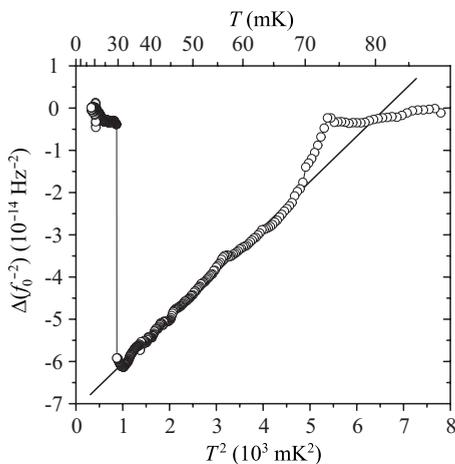(9)

with all factors being measured.

FIG. 12. Difference of the inverse squares of fork resonance frequencies during warming and cooling in the measurement at 11 bar, plotted as a function of T^2 to find the coefficient β of the quadratic temperature dependence of the saturation concentration. The cornerlike feature at higher temperatures is produced by the second sound resonance at about 80 mK seen in Fig. 11 as the first small loop.
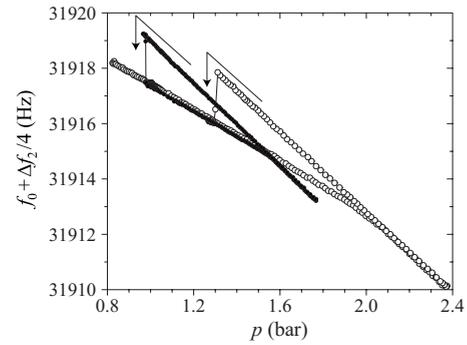

FIG. 13. Fork data at 10 mK during pressure sweeps with two different amounts of ^{3}He. The arrows indicate the fall from the supersaturated state due to decreasing pressure.

B. Pressure sweep

The pressure sweep procedure proved applicable below about 8 bar, where the pressure dependence of the saturation concentration is fairly steep. To perform the measurement, we first raised the pressure of a phase-separated mixture slowly at a constant temperature T by adding ^{4}He until the pure ^{3}He phase disappeared as a result of the increase in solubility. This event was indicated by a kink in both the resonance width and the frequency of the fork. After that, we started lowering the pressure to confirm the point of total mixing. Below that point the mixture entered the metastable supersaturated state and remained there down to a somewhat lower pressure where the pure ^{3}He phase nucleated and the initial phase-separated situation was restored.

An example of the pressure sweep measurements, where the fork response versus pressure at 10 mK is shown with two different amounts of ^{3}He, is seen in Fig. 13. At low pressures, the two data sets follow the same curve corresponding to the saturated mixture and turn at a certain pressure to an intersecting steeper curve corresponding to a mixture that contains all the ^{3}He in the cell. The intersection point gives the pressure p at which the solubility at T equals the concentration determined by the ^{3}He content in question through Eq. (4). We obtain the desired factor as

$$\beta(p) = T^{-2}\left[\frac{x_s(p,T)}{x_s(p,0)} - 1\right],$$
(10)

viable in the range 30–70 mK. At lower temperatures the difference is too small to be reliably observed, and at higher temperatures the second sound effects complicate the situation. Also, the quadratic temperature dependence is not expected to hold much further than that. The zero-temperature solubility at the arbitrary pressure p is evaluated by an interpolation of our data. Only relative values are needed here so that the accuracy does not suffer from uncertainty in the absolute solubility.

C. Results

All relevant data are collected to Fig. 14 presenting the temperature-dependence factor β measured by our two methods together with some earlier results. The graph also shows
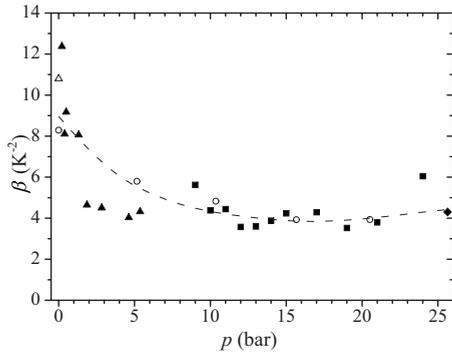
FIG. 14. Temperature-dependence factor of the saturation concentration. Our data: (■) temperature sweeps, (▲) pressure sweeps, and (◆) melting pressure. Comparison: (△) Edwards' data (Ref. 28) and (○) Yorozu's data (Ref. 7). The dashed line is a guide to the eye.

one data point based on our measurements on the concentration and temperature dependence of the melting pressure of ^{4}He in the mixture. The accuracy of our results on the temperature dependence is only modest, mainly because of the disturbing influence of the second sound resonances, but they are in good agreement with the previously published values of β.[7,28] After the initial drop of this coefficient at low pressures, it has little pressure dependence. The question whether it eventually starts to increase at the highest pressures still remains, as the scatter of our data does not allow a firm conclusion on that.

VI. DISCUSSION

We took over to examine the solubility of ^{3}He in ^{4}He at the highest possible pressures in the liquid phase because we are conducting cooling experiments at the crystallization pressure. Prior to this work there was no proper determination of the saturation concentration at the melting curve; only some scattered estimates and unreliable extrapolations could be found in the literature. Without knowing the saturation concentration with reasonable accuracy, there is no way of making proper analysis of any other phenomena encountered in the experiments on helium mixtures.

Admittedly, our experimental arrangement was not fully optimized for this kind of study. The integration with the ultrasensitive capacitive pressure transducer made the cell geometry unnecessarily complicated and the presence of several superleak lines multiplied the concern of them altering the simple situation with a well defined volume of the experimental cell. These components were there because the main purpose was to test their performance for the adiabatic melting experiment.

In retrospect, a quartz fork with somewhat smaller dimensions would probably have performed better in this experiment by producing more clean data in mixtures at higher temperatures because of reduced effects of second sound. We chose the "big one" instead of the smaller one, which is also available, because it performed more nicely in the tests in vacuum at 4 K. There was clearly better linearity with much higher oscillation amplitudes and essentially no internal

damping. The problems with the small forks from the same manufacturer were probably due to less perfect quartz crystal used in their production. Another indication of this was that the resonance frequency of the small forks drifted at room temperature if exposed to helium atmosphere at moderate pressures (say, 10 bar), whereas the other forks did not show such behavior. This is interpreted as the material having had lattice imperfections through which the helium atoms diffused into the quartz crystal.[29] Under normal conditions, the diffusion of He into single-crystal quartz should be extremely slow. However, for the measurements on helium mixtures at very low temperatures, such problems should have had no significance, since the damping due to ^{3}He quasiparticles overwhelms any such imperfection. The anomalies due to the second sound resonances at intermediate temperatures could not be foreseen.

Besides the main theme of this article, we have demonstrated some other mixture phenomena, which obviously deserve some further attention. For example, the process of the nucleation of the pure ^{3}He phase from the supersaturated condition (regularly produced in the course of these experiments) seems very interesting indeed. Although the pure phase must eventually find its way to the top of the experimental cell, which in our case was quite far from the main volume and from the observation probe and, moreover, separated from that by a relatively narrow path in between (see Fig. 1), the equilibrium phase-separated condition was restored rather rapidly at the site of the fork after the event of nucleation. The data points in Figs. 11 and 13 were taken with an interval of a couple of seconds, and yet there are merely a few or none data points indicating the system being switching between the two conditions. We are probably dealing with quite an exceptional macroscopic quantum nucleation process here.[30] Although such a phase transition must be statistical from the outset, there were some regularities in the behavior.

A. ^{3}He content of the cell

Let us finally elaborate on the validity of our concept of taking care of the ^{3}He balance in our experiment, as knowing the precise amount of ^{3}He in the cell at every stage of the experiment is crucial for the calibration of the fork as a ^{3}He density gauge in mixtures. As the time span between the first and the last addition of ^{3}He was over a hundred days and both the filling lines of the cell were open to room-temperature parts most of the time, we have to take into account the possibility of loss of ^{3}He. On the grounds of fork measurements, it appeared that there was no observable continuous loss, but, on the other hand, a couple of distinct events of a slight drop in the ^{3}He content occurred, apparently during the time spent at the melting curve of the mixture. Therefore, it was necessary to verify the values of the ^{3}He content afterwards. After the actual experiment, we emptied the cell above 4 K, filled it again first with ^{4}He, and repeated the ^{3}He addition in just two days, making only the measurements necessary for comparing the ^{3}He concentration with the actual experiment.

The data used for the ^{3}He content comparison are presented in Fig. 15. The upper graph plots width of the fork
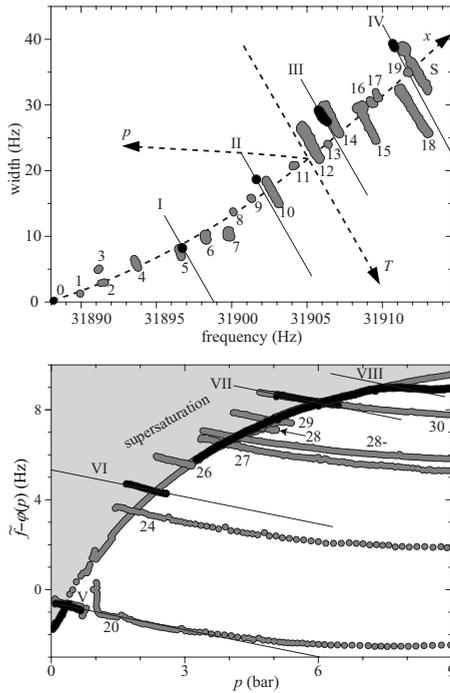
FIG. 15. Quartz fork data used to determine the amount of ^{3}He in the cell. Gray points, labeled with Arabic numerals, are from the actual experiment, and black ones, labeled with Roman numerals, from the fast reference dosing. The upper graph presents measurements at saturated vapor pressure, below and at the solubility limit "S," obtained at 10 mK or during temperature sweeps around that value. The lower graph shows results at elevated pressures in terms of the pressure dependence of the difference of $\widetilde{f}$ and a function $\varphi(p)$ (see text). The parallel lines drawn through the reference data V–VIII are examples of fits used to compare the ^{3}He contents.

FIG. 16. The dependence of the fork response on the cumulative amount of ^{3}He in the cell N_3, based on the data shown in Fig. 15. Upper graph: the values of $\widetilde{f}$ at SVP up to the saturation limit, and a linear fit to the data from the reference dosing. Lower graph: heights of fitted lines parallel to those shown in the lower graph of Fig. 15 at $p = 7$ bar, which was chosen as the criterion for comparing ^{3}He contents exceeding the saturation limit at SVP. The horizontal distance from the line defined by the reference doses (black points) gives the loss of ^{3}He during the actual experiment (gray points).

resonance versus frequency and covers ^{3}He contents below the amount needed to saturate the mixture at the saturated vapor pressure (SVP). The dashed x-, T-, and p-axes sketch the change in the fork response by increasing concentration, temperature, and pressure. The lower graph shows the data for the amounts above the SVP saturation limit. It plots the pressure dependence of the expression $\widetilde{f} - \varphi(p)$, where $\varphi(p) = [263.1 \exp(-p/36.85 \text{ bar}) + 31\,660]$ Hz, chosen for plotting purposes to emphasize the effect of concentration. The ascending trace corresponds to saturation concentration, increasing as a function of pressure, and the intersecting traces to homogeneous mixtures of different ^{3}He contents, supersaturated when in the shaded region above the saturation curve. The irregular features between 0.5 and 1 bar result from the difficulty to cross that pressure range smoothly and to measure the cell pressure accurately by the gauge outside the cryostat, as the crossing involves a relatively large flow of ^{4}He to either fill or empty the capillaries between the cell and the 4 K bath.

From the data presented in Fig. 15 we extracted a characteristic frequency to indicate the amount of ^{3}He at each number of added doses. Below saturation, at SVP, a natural choice is the zero viscosity frequency $\widetilde{f}$, whereas for the ^{3}He contents that dissolve only at elevated pressures, we fit parallel lines in the lower graph to the homogeneous mixture
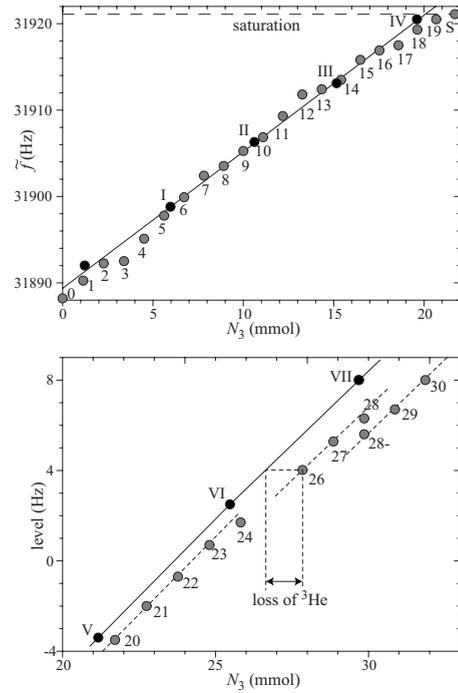
data at the points where they cross the saturation curve and we use the heights of those lines at 7 bar as characteristic frequencies. Strictly speaking, these frequencies are not exactly linear in the amount of ^{3}He, but in this comparison of amounts close to each other, the higher-order corrections are negligible. Figure 16 presents the obtained data and lines defined by the reference measurements, which enable the detection of the loss of ^{3}He at each stage of the actual experiment by simply measuring the horizontal distance of the data point from the reference line. When doses were added basically one after the other, as 20–23, 26–27, and 29–30, they connect with a line (dashed lines in the graph) parallel with that of the reference dosing, reassuring the validity of the comparison.

The amount of ^{3}He added at a time decreased steadily from the first 1.15 mmol dose to 0.995 mmol in the 30th dose because the pressure of the source of ^{3}He naturally kept decreasing. In total the first 30 doses amounted to 31.9 mmol. Figure 17 shows a plot of the calculated loss as a function of the number of ^{3}He doses added. The hollow squares represent the results obtained at the saturated vapor pressure and are somewhat scattered because at the SVP, it was possible that the cell was not completely full of liquid but there could also have been a vapor phase (essentially vacuum) present, which enhances the ^{3}He concentration de-
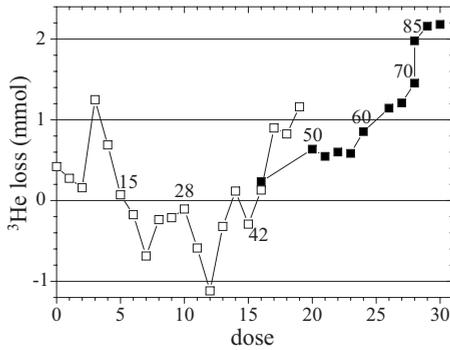
FIG. 17. Loss of ^{3}He from the cell calculated by comparison between fork responses during the actual experiment and the fast ^{3}He addition. The numbers refer to days after the first ^{3}He addition. □: zero pressure; ■: elevated pressure.

tected by the fork. It was possible to keep depleting the cell from ^{4}He, although the vapor pressure is practically zero at millikelvin temperatures, because the upper end of the superleak always had a pressure of 0.1–0.2 bar due to the fountain pressure of superfluid ^{4}He. This problem was not fully acknowledged at the beginning of the experiment, when most of the time was spent at SVP. Moreover, for the first few doses, there is some temperature and concentration dependence in the second sound velocity still at 10 mK and it may be that the irregular behavior, especially for dose three, is due to a nearby second sound resonance. The solid squares represent results obtained by comparing the fork responses at elevated pressures.

Because the true value of the loss cannot decrease, we conclude that, within the achieved accuracy, there was no significant loss before the 16th dose. However, after the measurements with 30 doses, some 7.4% of the total amount of added ^{3}He had exited the cell at some point. Before adding the 29th dose, the cell was cooled below the superfluid transition of ^{3}He, when some pure ^{3}He liquid had been made to appear by creating some solid ^{4}He in the cell. At that time we encountered the largest single event of loss of ^{3}He from the system, appearing in Fig. 15 as the difference between the data labeled "28" and "28-," obtained before and after, respectively, the low-temperature experiments. The other smaller events had no obvious reason but, nevertheless, their influence to the ^{3}He balance has been taken into account when compiling the plot in Fig. 7.

VII. SUMMARY

Dilute mixtures of ^{3}He in ^{4}He continue to present both theoretical and experimental challenges as exceptional sys-

tems of quantum fluids with components obeying different quantum statistics governing their behavior at very low temperatures. So far helium mixtures have been cooled to temperatures somewhat below 0.1 mK,[31,32] with no indication of superfluidity of the dilute ^{3}He; the theoretical predictions of the transition temperature range over several orders of magnitude, the highest estimates lying in the range of tens of microkelvins. Both theoretically and experimentally, the concentration of the saturated helium mixture is a crucial factor in such investigations. Accordingly, we studied helium mixtures in the millikelvin regime across the whole pressure range from zero to the melting pressure of the mixture, probing the sample by a vibrating quartz tuning fork.

Measurement of the concentration of ^{3}He in liquid helium mixtures by a quartz tuning fork is an application of this emerging tool for low-temperature helium research. It is based on the dependence of the resonance frequency of the fork on the density of the liquid and to the known relations of that density to pressure and concentration. We have successfully utilized this method to study helium mixtures at millikelvin temperatures, extending the measurements of the zero-temperature saturation concentration for the first time across the whole accessible pressure range, and finding the quadratic temperature coefficient of the solubility by exploiting supersaturation. The fork turned out to be a highly sensitive, reliable, and reproducible detector of the density, and thereby of the pressure and the ^{3}He concentration, of the mixtures.

The dependence of the resonance frequency of the fork on the density of helium liquids is nearly what one expects by simple arguments; the deviation is explicable by the compressibility of the fluid, in other words, by the fact that the oscillator produces sound in the liquid. In addition to ordinary sound in mixtures, it also excites second sound or concentration waves whose wavelength falls in the length scale of our fork at the applied frequencies. This gives rise to second sound resonances, which complicate the precise concentration measurements, but, on the other hand, may be useful for studying other properties of the mixtures.

*epentti@boojum.hut.fi

[1] E. R. Dobbs, *Helium Three* (Oxford University Press, New York, 2000).
[2] A. P. Sebedash, JETP Lett. **65**, 276 (1997).
[3] A. P. Sebedash, J. T. Tuoriniemi, S. T. Boldarev, E. M. M. Pentti, and A. J. Salmela, J. Low Temp. Phys. **148**, 725 (2007).
[4] R. I. Schermer, L. Passell, and D. C. Rorer, Phys. Rev. **173**, 277 (1968).

[5] G. E. Watson, J. D. Reppy, and R. C. Richardson, Phys. Rev. **188**, 384 (1969).

[6] J. Landau, J. T. Tough, N. R. Brubaker, and D. O. Edwards, Phys. Rev. A **2**, 2472 (1970).

[7] S. Yorozu, M. Hiroi, H. Fukuyama, H. Akimoto, H. Ishimoto, and S. Ogawa, Phys. Rev. B **45**, 12942 (1992).

[8] K. Hatakeyama, S. Noma, E. Tanaka, S. N. Burmistrov, and T. Satoh, Phys. Rev. B **67**, 094503 (2003).

[9] D. O. Clubb, O. V. L. Buu, R. M. Bowley, R. Nyman, and J. R. Owers-Bradley, J. Low Temp. Phys. **136**, 1 (2004).

[10] R. Blaauwgeers *et al.*, J. Low Temp. Phys. **146**, 537 (2007).

[11] J. T. Tough, W. D. McCormick, and J. G. Dash, Phys. Rev. **132**, 2373 (1963).

[12] D. C. Carless, H. E. Hall, and J. R. Hook, J. Low Temp. Phys. **50**, 583 (1983).

[13] H. A. Nichol, L. Skrbek, P. C. Hendry, and P. V. E. McClintock, Phys. Rev. Lett. **92**, 244501 (2004).

[14] K. Gloos, W. Schoepe, J. T. Simola, and J. T. Tuoriniemi, Cryogenics **32**, 791 (1992).

[15] E. Collin, L. Filleau, T. Fournier, Y. M. Bunkov, and H. Godfrin, J. Low Temp. Phys. **150**, 739 (2008).

[16] A. Sebedash, J. T. Tuoriniemi, S. Boldarev, E. M. M. Pentti, and A. J. Salmela, *24th International Conference on Low Temperature Physics-LT24*, AIP Conf. Proc. No. 850 (AIP, New York, 2006), p. 1591.

[17] E. Pentti, J. Tuoriniemi, A. Salmela, and A. Sebedash, J. Low Temp. Phys. **146**, 71 (2007).

[18] Fox Electronics, Fort Myers, Florida, USA, http://www.foxonline.com

[19] E. M. Pentti, J. T. Tuoriniemi, A. J. Salmela, and A. P. Sebedash, J. Low Temp. Phys. **150**, 555 (2008).

[20] J. Bardeen, G. Baym, and D. Pines, Phys. Rev. **156**, 207 (1967).

[21] E. Tanaka, K. Hatakeyama, S. Noma, and T. Satoh, Cryogenics **40**, 365 (2000).

[22] J. C. King and H. A. Fairbank, Phys. Rev. **93**, 21 (1954).

[23] H. Brucker, Y. Disatnik, and R. Meyuhas, J. Low Temp. Phys. **24**, 193 (1976).

[24] N. R. Brubaker, D. O. Edwards, R. E. Sarwinski, P. Seligmann, and R. A. Sherlock, J. Low Temp. Phys. **3**, 619 (1970).

[25] M. Kollar and D. Vollhardt, Phys. Rev. B **61**, 15347 (2000).

[26] D. Einzel and J. M. Parpia, J. Low Temp. Phys. **109**, 1 (1997).

[27] J. Martikainen, J. Tuoriniemi, T. Knuuttila, and G. Pickett, J. Low Temp. Phys. **126**, 139 (2002).

[28] D. O. Edwards, E. M. Ifft, and R. E. Sarwinski, Phys. Rev. **177**, 380 (1969).

[29] T. S. Argunova, L. M. Sorokin, B. Z. Pevzner, J. H. Je, Y. Hwu, and W.-L. Tsai, J. Phys. D **36**, A12 (2003).

[30] E. Tanaka, K. Hatakeyama, S. Noma, S. N. Burmistrov, and T. Satoh, J. Low Temp. Phys. **127**, 81 (2002).

[31] G.-H. Oh, Y. Ishimoto, T. Kawae, M. Nakagawa, O. Ishikawa, T. Hata, and T. Kodama, J. Low Temp. Phys. **95**, 525 (1994).

[32] J. Tuoriniemi, J. Martikainen, E. Pentti, A. Sebedash, S. Boldarev, and G. Pickett, J. Low Temp. Phys. **129**, 531 (2002).